C^1 continuous h-Adaptive Least-Squares Spectral Element Method for Phase-Field Models

Keunsoo Park[a,b], Marc Gerristma[b], Maria Fernandino[a]

[a] *Department of Energy and Process Engineering, Norwegian University of Science and Technology, N-7491 Trondheim, Norway*
[b] *Aerospace Engineering, Delft University of Technology, Kluyverweg 1, Delft, The Netherlands*

Abstract

The phase-field method has been successfully modeled the interface dynamics in multiphase flow phenomena. However, there has been a great disjunction in the interface thickness between in reality and in numerics due to the high gradient of solutions within the interfacial region. By using finer mesh on the interface and coarser mesh in the rest of computational domain, the phase-field method can handle larger scale of problem with realistic length of interface. In this work, a C^1 continuous h-adaptive mesh refinement technique with the least-squares spectral element method for the Navier-Stokes-Cahn-Hilliard (NSCH) system and the isothermal Navier-Stokes-Korteweg (NSK) system is presented. Hermite polynomials are used to give global differentiability in the approximated solution, and a space-time coupled formulation and the element-by-element technique are implemented. Two refinement strategies based on the solution gradient and the local error estimators are suggested and they are compared through two numerical examples.

Keywords: Adaptive mesh; Least-squares; Hermite polynoials; Cahn-Hilliard; Korteweg; Phase-field

1. Introduction

The models in the phase-field method contain the convection-diffusion equations for the phase–field parameter. They can prohibit the necessity of tracking the interface, and provide a thermodynamically consistent formulation for interfacial surface tension from their own free energy functions [1, 2]. Among the phase-field models, the Cahn-Hilliard equation [3] and the Korteweg type equation [4] have been widely applied to a range of droplet dynamics [5], binary polymer mixtures [6, 7] and dendritic growth [8]. The Cahn-Hilliard equation can be coupled with the Navier-Stokes equation to take hydrodynamic effects

Email address: keunsoo.park@ntnu.no/whwr0428@gmail.com (Keunsoo Park)

into consideration, resulting in the Navier-Stokes-Cahn-Hilliard (NSCH) system, so-called Model H [9]. Based on the van der Waals fluid model, Korteweg [10] developed a model of the capillary stress tensor, and added the tensor into the momentum equation, resulting the Navier-Stokes-Korteweg (NSK) system.

It is known that the thickness of the interface between immiscible liquids is in the order of tens of nanometers [11]. However, there is a practical limitation on the phase-field method to describe such thin interface. In the phase-field method, the mesh is required to be sufficiently fine, since the order parameter has a steep gradient within the interfacial region [12]. For instance, the Cahn-Hilliard equation introduces the Cahn number, which is a ratio of the interface thickness to the characteristic length of discretization. Typically 0.01 to 0.04 of the Cahn number is used by controlling mesh size with respect to the interface length [13]. Due to this limitation, most of numerical studies with the phase-field method have been conducted on small-scale systems where the numerical interface thickness is assumed to be of the same order of magnitude as the real interface in the nature. Nevertheless, for larger problem where the droplet size is much larger than the physical value of the interface thickness or for the flow with the temperature far from the critical temperature, there has been a great disparity between the numerical interface thickness and the macroscopic scale, since capturing the real interfacial thickness is not numerically acceptable.

Our solver based on the least-squares formulation with a spectral approximation has succeeded in solving several phase-field models [14, 15]. The least-squares formulation gives the symmetric positiveness and circumvents the LBB condition, and a higher order accuracy is provided at the narrow interfacial region from the spectral methods [16]. The adaptive mesh enables the least-squares spectral element method to deal with the phase-field models more efficiently by assigning finer elements within narrow diffuse interfaces and coarser elements in pure phases. More information on the least-squares finite element schemes can be found in [17] and on the mathematical background of adaptive algorithm in [18].

In the present work, we apply a high-order h-adaptive mesh refinement technique on the least-squares spectral element formulation. C^1 Hermite tricubic bases are used, and to provide C^1 continuity between geometrically non-conforming neighboring elements, the hanging-node constraints suggested by Stogner et al. [19], but expressed in the least-squares manner by us, are used. Two refinement criteria based on the gradient of phase parameter and the local error estimators are used to flag which elements need to be refined or to be coarsened. Simulation results are computed using both uniform high-resolution meshes and adaptive meshes for comparison purposes. To the authors' best knowledge, our work is the first C^1 continuous adaptive scheme onto the least–squares method.

The rest of the present paper is organized as follows. Section 2 presents a least-squares spectral element formulation of the NSCH and the isothermal NSK system. In Section 3, the C^1 continuous h-refinement technique adapted into the least-squares scheme is presented. New data structures and the refinement strategies for a transient problem can be found in Section 4. The results and

discussion with the simulation of coalescence driven by two phase-field models are in Section 5. We draw conclusion in Section 6.

2. The mathematical formulation

2.1. The governing equations

We define the space-time set $\Omega := \Omega_{\mathbf{x}} \times (0, T), T > 0$, for a two-dimensional open domain $\Omega_{\mathbf{x}} \in \mathbb{R}^2$. The spatial boundary of Ω is denoted as $\Gamma := \partial\Omega_{\mathbf{x}} \times (0, T)$. For a flow of two immiscible, incompressible and viscous fluids, the dimensionless NSCH system can be stated as follows: find the unknowns $\boldsymbol{u} = \boldsymbol{u}(\boldsymbol{x}, t) : \Omega \to \mathbb{R}^2$, $P = P(\boldsymbol{x}, t) : \Omega \to \mathbb{R}$, $C = C(\boldsymbol{x}, t) : \Omega \to (0, 1)$ and $\omega = \omega(\boldsymbol{x}, t) : \Omega \to \mathbb{R}$ such that

$$\nabla \cdot \boldsymbol{u} = 0 \qquad \text{in } \Omega, \tag{1}$$

$$\frac{\partial \boldsymbol{u}}{\partial t} + \boldsymbol{u}\nabla \cdot \boldsymbol{u} + \nabla P - \frac{1}{Re}\nabla \cdot \left(\nabla \boldsymbol{u} + \nabla \boldsymbol{u}^T\right) - \frac{1}{ReCa}\omega \nabla C = 0 \qquad \text{in } \Omega, \tag{2}$$

$$\frac{\partial C}{\partial t} + \boldsymbol{u} \cdot \nabla C - \frac{1}{Pe}\nabla^2 \omega = 0 \qquad \text{in } \Omega, \tag{3}$$

$$\omega = C^3 - 1.5C^2 + 0.5C - Cn^2\nabla^2 C \qquad \text{in } \Omega, \tag{4}$$

$$\boldsymbol{u}(\boldsymbol{x}, 0) = \boldsymbol{u}_0(\boldsymbol{x}), \quad C(\boldsymbol{x}, 0) = C_0(\boldsymbol{x}) \qquad \text{in } \Omega_{\mathbf{x}}, \tag{5}$$

$$\boldsymbol{u} = 0, \quad \nabla C \cdot \mathbf{n} = 0, \quad \nabla \omega \cdot \mathbf{n} = 0 \qquad \text{on } \Gamma. \tag{6}$$

Here $\boldsymbol{u}$ is the velocity field, P the pressure, w the chemical potential, and M the mobility.

For a compressible two-phase flow based on the van der Waals fluid model, the dimensionless isothermal NSK system can be stated as follows: find the unknowns $\rho = \rho(\boldsymbol{x}, t) : \Omega \to \mathbb{R}$, $\boldsymbol{u} = \boldsymbol{u}(\boldsymbol{x}, t) : \Omega \to \mathbb{R}^2$ and $\varphi = \varphi(\boldsymbol{x}, t) : \Omega \to \mathbb{R}$ such that

$$\frac{\partial \rho}{\partial t} + \nabla \cdot (\rho \boldsymbol{u}) = 0 \qquad \text{in } \Omega, \tag{7}$$

$$\begin{aligned} &\rho\left(\frac{\partial \boldsymbol{u}}{\partial t} + \boldsymbol{u}\nabla \cdot \boldsymbol{u}\right) + \left[\frac{24}{(3-\rho)^2} - 6\rho\right]\nabla\rho \\ &- \frac{1}{Re}\nabla \cdot \left(\nabla \boldsymbol{u} + \nabla \boldsymbol{u}^T - \frac{2}{3}\nabla \cdot \boldsymbol{u}\mathbf{I}\right) - \frac{1}{We}\rho\nabla\varphi = 0 \end{aligned} \qquad \text{in } \Omega, \tag{8}$$

$$\nabla^2 \rho - \varphi = 0 \qquad \text{in } \Omega, \tag{9}$$

$$\rho(\boldsymbol{x}, 0) = \rho_0(\boldsymbol{x}), \quad \boldsymbol{u}(\boldsymbol{x}, 0) = \boldsymbol{u}_0(\boldsymbol{x}) \qquad \text{in } \Omega_{\mathbf{x}}, \tag{10}$$

$$\nabla\rho \cdot \mathbf{n} = 0, \quad \boldsymbol{u} = 0 \qquad \text{on } \Gamma \tag{11}$$

where ρ is the density, and φ is an auxiliary variable to reduce the differential order of system from third to second.

The dimensionless numbers used in (1)-(11) are Reynold number Re, Capillary number Ca, Peculet number Pe, Cahn number Cn and Weber number We, and they are formulated as:

$$\begin{aligned} &Re = \frac{\rho_0 U_0 L_0}{\mu}, \quad Ca = \frac{\mu U_0}{\sigma}, \quad Pe = \frac{L_0 U_0}{M}, \quad Cn = \frac{\epsilon}{L_0}, \\ &We = \frac{L_0^2 U_0^2}{K \rho_0} = \frac{\rho_0 U_0^2 L_0}{\sigma}, \end{aligned} \tag{12}$$

where ρ_0, U_0, L_0 are the reference density, velocity and length, μ the viscosity, σ the surface tension, ϵ the interfacial parameter and K the capillary coefficient. The derivation and the physical meaning of the NSCH system and the isothermal NSK system are explained in our previous studies [14] and [15] in more detail.

2.2. Least-squares method

The system (1)-(6) can be viewed as the coupled Navier-Stokes and Cahn-Hilliard equations, and in the decoupling of those two equations we use a relaxation method to assure convergence and to accelerate the iteration. And the Newton linearization method is used to cope with nonlinear terms in the governing equations. The terms from previous decoupling step are denoted as subscript n, and the terms from the previous linearization step are denoted as subscript l. For the Navier-Stokes system for a two-dimensional spatial domain, the set of partial differential equation with the unknown $\mathbf{u}_{NS}^T = [u\ v\ P]$ can be represented as

$$\frac{\partial u}{\partial x} + \frac{\partial v}{\partial y} = 0, \tag{13}$$

$$\begin{aligned} &\left[\left(\frac{\partial}{\partial t} + u_l \frac{\partial}{\partial x} + v_l \frac{\partial}{\partial y} + \frac{\partial u}{\partial x}\Big|_l\right) - \frac{1}{Re}\left(\frac{\partial^2}{\partial x^2} + \frac{\partial^2}{\partial y^2}\right)\right] u + \frac{\partial u}{\partial y}\Big|_l v + \frac{\partial P}{\partial x} \\ &= u_l \frac{\partial u}{\partial x}\Big|_l + v_l \frac{\partial u}{\partial y}\Big|_l + \frac{1}{ReCa}\omega_n \frac{\partial C}{\partial x}\Big|_l, \end{aligned} \tag{14}$$

$$\begin{aligned} &\frac{\partial v}{\partial x}\Big|_l u + \left[\left(\frac{\partial}{\partial t} + u_l \frac{\partial}{\partial x} + v_l \frac{\partial}{\partial y} + \frac{\partial v}{\partial y}\Big|_l\right) - \frac{1}{Re}\left(\frac{\partial^2}{\partial x^2} + \frac{\partial^2}{\partial y^2}\right)\right] v + \frac{\partial P}{\partial y} \\ &= \frac{\partial v}{\partial x}\Big|_l + v_l \frac{\partial v}{\partial y}\Big|_l + \frac{1}{ReCa}\omega_n \frac{\partial C}{\partial y}\Big|_l, \end{aligned} \tag{15}$$

In the same manner, for the Cahn-Hilliard system for a two-dimensional spatial domain, the set of partial differential equations with the unknowns $\mathbf{u}_{CH}^T = [C\ \omega]$

can be represented as

$$\left[\frac{\partial}{\partial t}+u_n\frac{\partial}{\partial x}+v_n\frac{\partial}{\partial y}\right]C-\frac{M}{Pe}\left(\frac{\partial^2}{\partial x^2}+\frac{\partial^2}{\partial y^2}\right)\omega=0, \tag{16}$$

$$\left[3C_l^2-3C_l+0.5-Cn^2\left(\frac{\partial^2}{\partial x^2}+\frac{\partial^2}{\partial y^2}\right)\right]C-\omega=2C_l^3-1.5C_l^2. \tag{17}$$

For the isothermal NSK system for a two-dimensional spatial domain, the set of partial differential equation with the unknown $\mathbf{u}_K^T=[\rho\ u\ v\ \varphi]$ can be represented as

$$\begin{aligned}&\left[\frac{\partial}{\partial t}+u_l\frac{\partial}{\partial x}+v_l\frac{\partial}{\partial y}+\frac{\partial u_l}{\partial x}+\frac{\partial v_l}{\partial y}\right]\rho+\left[\rho_l\frac{\partial}{\partial x}+\frac{\partial\rho_l}{\partial x}\right]u\\&+\left[\rho_l\frac{\partial}{\partial y}+\frac{\partial\rho_l}{\partial y}\right]v=u_l\frac{\partial\rho_l}{\partial x}+\rho_l\frac{\partial u_l}{\partial x}+v_l\frac{\partial\rho_l}{\partial y}+\rho_l\frac{\partial v_l}{\partial y},\end{aligned} \tag{18}$$

$$\begin{aligned}&\left[\left(\frac{24}{(3-\rho_l)^2}-6\rho_l\right)\frac{\partial}{\partial x}+\left(\frac{\partial u_l}{\partial t}+u_l\frac{\partial u_l}{\partial x}+v_l\frac{\partial u_l}{\partial y}-\frac{1}{We}\frac{\partial\varphi_l}{\partial x}\right)\right]\rho\\&+\left[\rho_l\left(\frac{\partial}{\partial t}+u_l\frac{\partial}{\partial x}+v_l\frac{\partial}{\partial y}\right)-\frac{1}{Re}\left(\frac{4}{3}\frac{\partial^2}{\partial x^2}+\frac{\partial^2}{\partial y^2}\right)+\rho_l\frac{\partial u_l}{\partial x}\right]u\\&+\left[\rho_l\frac{\partial u_l}{\partial y}-\frac{1}{3Re}\frac{\partial^2}{\partial x\partial y}\right]v-\frac{1}{We}\rho_l\frac{\partial\varphi}{\partial x}\\&=\rho_l\frac{\partial u_l}{\partial t}+2\rho_l u_l\frac{\partial u_l}{\partial x}+2\rho_l v_l\frac{\partial u_l}{\partial y}-\frac{1}{We}\rho_l\frac{\partial\varphi_l}{\partial x},\end{aligned} \tag{19}$$

$$\begin{aligned}&\left[\left(\frac{24}{(3-\rho_l)^2}-6\rho_l\right)\frac{\partial}{\partial y}+\left(\frac{\partial v_l}{\partial t}+u_l\frac{\partial v_l}{\partial x}+v_l\frac{\partial v_l}{\partial y}-\frac{1}{We}\frac{\partial\varphi_l}{\partial y}\right)\right]\rho\\&+\left[\rho_l\frac{\partial v_l}{\partial x}-\frac{1}{3Re}\frac{\partial^2}{\partial x\partial y}\right]u+\left[\rho_l\left(\frac{\partial}{\partial t}+u_l\frac{\partial}{\partial x}+v_l\frac{\partial}{\partial y}\right)\right.\\&\left.-\frac{1}{Re}\left(\frac{\partial^2}{\partial x^2}+\frac{4}{3}\frac{\partial^2}{\partial y^2}\right)+\rho_l\frac{\partial v_l}{\partial y}\right]v-\frac{1}{We}\rho_l\frac{\partial\varphi}{\partial y}\\&=\rho_l\frac{\partial v_l}{\partial t}+2\rho_l u_l\frac{\partial v_l}{\partial x}+2\rho_l v_l\frac{\partial v_l}{\partial y}-\frac{1}{We}\rho_l\frac{\partial\varphi_l}{\partial y},\end{aligned} \tag{20}$$

$$\left[\frac{\partial^2}{\partial x^2}+\frac{\partial^2}{\partial y^2}\right]\rho-\varphi=0. \tag{21}$$

For both equation sets, the final system with the boundary conditions included can be expressed in general as

$$\mathcal{L}\mathbf{u}=\mathcal{G} \qquad \text{in } \Omega, \tag{22}$$

$$\mathcal{B}\mathbf{u}=\mathbf{u}_\Gamma \qquad \text{on } \Gamma, \tag{23}$$

where $\mathcal{L}$ represents the partial differential operator, $\mathcal{G}$ the corresponding source term, $\mathcal{B}$ the boundary conditions operator, and $\mathbf{u}_\Gamma$ the specified values on the boundaries. In this work, the boundary conditions are incorporated into the least-squares functional so that they are also a part of the minimization problem, namely

$$\mathcal{J}(\mathbf{u}) = \frac{1}{2}\left\|\mathcal{L}\mathbf{u} - \mathcal{G}\right\|_{0,\Omega}^2 + \frac{1}{2}\left\|\mathcal{B}\mathbf{u} - \mathbf{u}_\Gamma\right\|_{0,\Omega}^2, \tag{24}$$

or equivalently,

Find $\mathbf{u} \in X(\Omega)$ such that

$$\mathcal{A}(\mathbf{u}, \mathbf{v}) = \mathcal{F}(\mathbf{v}) \qquad \forall \mathbf{v} \in X(\Omega), \tag{25}$$

with

$$\mathcal{A}(\mathbf{u}, \mathbf{v}) = (\mathcal{L}\mathbf{u}, \mathcal{L}\mathbf{v})_{0,\Omega} + (\mathcal{B}\mathbf{u}, \mathcal{B}\mathbf{v})_{0,\Gamma}, \tag{26}$$

$$\mathcal{F}(\mathbf{v}) = (\mathcal{G}, \mathcal{L}\mathbf{v})_{0,\Omega} + (\mathbf{u}_\Gamma, \mathcal{B}\mathbf{v})_{0,\Gamma}, \tag{27}$$

where $\mathcal{A} : X \times X \to \mathbb{R}$ is a symmetric, positive definite bilinear form and $\mathcal{F} : X \to \mathbb{R}$ a continuous linear form.

2.3. Spectral element discretization

The computational domain Ω is divided into Ne non-overlapping sub-domains Ω_e such that

$$\Omega = \sum_{e=1}^{Ne} \Omega_e, \qquad \Omega_i \cap \Omega_j = \emptyset, \quad i \neq j. \tag{28}$$

The discretization is based on a time-space coupled formulation with the time-stepping procedure. The solution is approximated on consecutively aligned space-time strips domains, and a strip is composed of only one element in time, $\Omega_e = \Omega_e^{\mathbf{x}} \times \Omega_e^t = (\mathbf{x}_e, \mathbf{x}_{e+1}) \times (t_n, t_{n+1})$ with the time step size $\Delta t = t_{n+1} - t_n$. Each sub-domain is mapped onto the unit cube $(\xi, \sigma, \eta) \in [-1, 1]^3$ for a two-dimensional spatial domain and one dimensional time domain, by an invertible mapping. A basis function for a two-dimensional space and time domain can be written as the tensor product of one-dimensional basis functions with the same order, i.e., $\mathbf{\Phi}_e^m(\xi, \varsigma, \eta) = \phi_e^i(\xi) \otimes \phi_e^j(\varsigma) \otimes \phi_e^k(\eta)$, with $m = i + j(p+1) + k(p+1)^2$ where $0 \leq i, j, k \leq p$. Thus, the local approximation $\mathbf{u}_e^h$ is expanded in $\mathbf{\Phi}$ continuous basis functions as

$$\mathbf{u}_e^h = \sum_{m=1}^{(p+1)^3} \mathbf{U}_e^m \mathbf{\Phi}_e^m, \tag{29}$$

with the expansion coefficient $\mathbf{U}_e^m$. The same basis functions and construction approach have been used in our previous study [14], and for more details we also refer [2, 21].

Together with integration by the Gaussian quadrature based on the GLL-roots, the discretization of the least-squares formulation (25) at an element-level can be expressed as

$$\mathbf{L}_e^T \mathbf{W}_e \mathbf{L}_e \mathbf{U}_e = \mathbf{L}_e^T \mathbf{W}_e \mathbf{F}_e, \tag{30}$$

where $\mathbf{L}$ is a matrix whose components are the evaluation of $\mathcal{L}$ with the Hermite polynomials at the quadrature points, and $\mathbf{F}$ is a vector of the evaluation of $\mathcal{G}$. $\mathbf{W}$ is a diagonal matrix of the quadrature weights, and in this article, the number of quadrature points Q are fixed at the same number of polynomial order of one dimensional basis function as $Q = p + 1$.

In this work, the discretized algebraic equation is solved by the element-by-element technique with the conjugated gradient method with the Jacobi preconditioner. A Matlab code developed at our group has been used as the main setup. For parallelization of the algorithm Matlab MPI is used to allocate the elements to processors and communicate between processors. The local solutions in all elements $\mathbf{u}_e^h$, are glued to construct the global approximation of solution $\mathbf{u}^h$, i.e.,

$$\mathbf{u}^h = \bigcup_{e=1}^{Ne} \mathbf{u}_e^h. \tag{31}$$

3. C^1 continuous h-refinement

Local mesh refinement is efficient, but it yields a non-conformal grid which could lead to discontinuities of the solution over the inter-element border. When the refinement levels of neighboring elements are different, the nodal basis of the coarser element, which have non-zero values on the inter-element border, are shared with the finer element. The non-conformal mesh for a two-dimensional case is illustrated in Figure 1, and nodal basis are shared on a non-conforming border γ - between Ω_1^0 and Ω_2^1 and between Ω_1^0 and Ω_4^1.

In this study, the spectral expansions are the same in all elements and a non-conformal mesh is obtained only by h-refinement. And since the grid refinement is applied to only spatial domain, we present the refinement technique only for a two-dimensional spatial domain. To ensure the global C^1 continuity in a non-conformal refinement, we introduce two L^2-norm least-squares functionals to be minimized for the value of solution, $\mathcal{J}_0^r$, and for the derivative of solution, $\mathcal{J}_1^r$, respectively, over the inter-element border γ between the finer element F and the coarser element C:

$$\mathcal{J}_0^r\left(\mathbf{u}_b^F; \mathbf{u}_b^C\right) = \int_\gamma \left(\mathbf{u}_b^F - \mathbf{u}_b^C\right)^2 d\mathrm{s}, \tag{32}$$

$$\mathcal{J}_1^r\left(\mathbf{u}_b^F; \mathbf{u}_b^C\right) = \int_\gamma \left(\nabla \mathbf{u}_b^F \cdot \mathbf{n} - \nabla \mathbf{u}_b^C \cdot \mathbf{n}\right)^2 d\mathrm{s}, \tag{33}$$

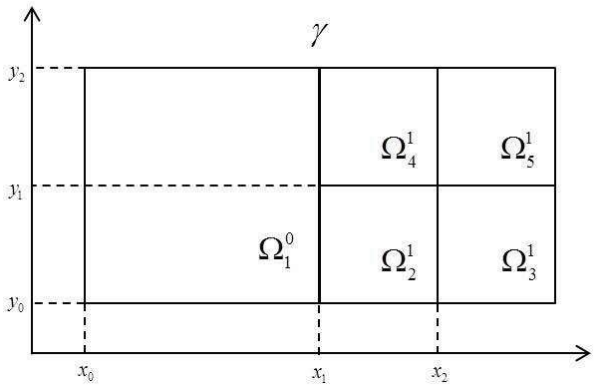

Figure 1: Non-conformal mesh in a two-dimensional domain.

where $\mathbf{u}_b$ is the solution on the inter-element border. Here, we explain the refinement formulation with an example configuration of elements where the non-conforming border is aligned to the y-axis, as depicted in Figure 1.

For this configuration, we define five linear coordinate transformations:

$$\begin{aligned}
&\mathcal{X}_0 : x^0(\xi) = \frac{x_1 - x_0}{2}\xi + \frac{x_1 + x_0}{2} && \xi \in [-1, 1], \\
&\mathcal{X}_1 : x^1(\xi) = \frac{x_2 - x_1}{2}\xi + \frac{x_2 + x_1}{2} && \xi \in [-1, 1], \\
&\mathcal{Y} : y(\eta) = \frac{y_2 - y_0}{2}\eta + \frac{y_2 + y_0}{2} && \eta \in [-1, 1], \\
&\mathcal{M}_m : \mu_m(\eta) = \frac{1}{2}(\eta - 1) && \eta \in [-1, 1], \\
&\mathcal{M}_p : \mu_p(\eta) = \frac{1}{2}(\eta + 1) && \eta \in [-1, 1],
\end{aligned} \tag{34}$$

(ξ, η) are the local coordinate of (x, y) in the parent element. The superscript 0 on x is for the element Ω_1^0 and 1 on x is for the lower refined-element Ω_2^1 and the upper refined-element Ω_4^1. μ_m and μ_p are auxiliary mapping variables on the border γ for Ω_2^1 and Ω_4^1, respectively.

The L^2-norm for the solution value on the border γ for Ω_2^1, denoted as $\mathcal{J}_{m,0}^r$ can be expressed as

$$\begin{aligned}
\mathcal{J}_{m,0}^r =& \int_{y_0}^{y_1} \left[\mathbf{u}_b^F(x, y) - \mathbf{u}_b^C(x, y)\right]^2 dy \\
=& \frac{y_1 - y_0}{2} \int_{-1}^{1} \left[\mathbf{u}_b^F\left(x^1(-1), y(\eta)\right) - \mathbf{u}_b^C\left(x^0(1), y\left(\mu_m(\eta)\right)\right)\right]^2 d\eta,
\end{aligned} \tag{35}$$

and $2/(y_1 - y_0)$ is the y-Jacobian for Ω_2^1, and it is denoted as $J_{y,1}$. With the basis functions aforementioned in Section 2, the approximation of $\mathbf{u}_b^F$ and $\mathbf{u}_b^C$

can be expressed as

$$\begin{aligned}\mathbf{u}_{b,h}^F\left(x^1(-1),y(\eta)\right)&=\sum_k u_{b,k}^F\phi_{1,i}(-1)\phi_{1,j}(\eta),\\ \mathbf{u}_{b,h}^C\left(x^0(1),y\left(\mu_m(\eta)\right)\right)&=\sum_k u_{b,k}^C\phi_{0,i}(1)\phi_{0,j}\left(\mu_m(\eta)\right),\end{aligned}\tag{36}$$

with $k=i+j(p+1)$ where $0\le i,j\le p$. The subscripts 0 and 1 on ϕ stand for the basis functions for Ω_1^0 and Ω_2^1, respectively. With the expansion coefficients $\mathbf{U}_{b,0}^F=[u_{b,k}^F]$ and $\mathbf{U}_{b,0}^C=[u_{b,k}^C]$, the minimization statement of $\mathcal{J}_{m,0}^r$ can be written in an algebraic form as

$$\nabla\mathcal{J}_{m,0}^r=0;\quad \mathbf{H}_{y,1}^T\mathbf{W}\mathbf{H}_{y,1}\mathbf{U}_{b,0}^F=\mathbf{H}_{y,1}^T\mathbf{W}\mathbf{H}_{ym,0}\mathbf{U}_{b,0}^C,\tag{37}$$

with

$$\begin{aligned}\left[\mathbf{H}_{y,1}\right]_{Q^2\times N}&=\phi_1(-1)\otimes\phi_1(\eta_q),\\ \left[\mathbf{H}_{ym,0}\right]_{Q^2\times N}&=\phi_0(1)\otimes\phi_0\left(\mu_m(\eta_q)\right),\quad q=1,...,Q,\end{aligned}\tag{38}$$

where Q is the number of quadrature points in either x- or y-axis, and $N=(p+1)^2$ is the number of basis functions in 2D. When $Q=p+1$, we can simplify Equation (37) by multiplying inverse matrices as

$$\mathbf{U}_{b,0}^F=\mathbf{H}_{y,1}^{-1}\mathbf{H}_{ym,0}\mathbf{U}_{b,0}^C\equiv\widetilde{\mathbf{Z}}_{m,0}\mathbf{U}_{b,0}^C,\tag{39}$$

with $\widetilde{\mathbf{Z}}_{m,0}$ the projection matrix for the solution value for the lower refined-element.

The expression for the derivative of solution can be obtained in a similar way. The L^2-norm for the derivative of the solution on the border γ for Ω_2^1, denoted as $\mathcal{J}_{m,1}^r$, can be expressed as

$$\begin{aligned}\mathcal{J}_{m,1}^r=&\int_{y_0}^{y_1}\left[\frac{\partial\mathbf{u}_b^F}{\partial x}(x^1,y)-\frac{\partial\mathbf{u}_b^C}{\partial x}(x^0,y)\right]^2dy\\ =&\frac{1}{J_{y,1}}\int_{-1}^{1}\left[\frac{\partial\xi}{\partial x^1}\frac{\partial\mathbf{u}_b^F}{\partial\xi}\left(x^1(-1),y(\eta)\right)-\frac{\partial\xi}{\partial x^0}\frac{\partial\mathbf{u}_b^C}{\partial\xi}\left(x^0(1),y\left(\mu_m(\eta)\right)\right)\right]^2d\eta,\end{aligned}\tag{40}$$

and $\partial\xi/\partial x^1$ and $\partial\xi/\partial x^0$ are the x-Jacobian for the mappings of $\mathcal{X}_1$ and $\mathcal{X}_0$, respectively. With the basis functions, the approximation of the x-derivatives of $\mathbf{u}_b^F$ and $\mathbf{u}_b^C$ can be expressed as

$$\begin{aligned}\frac{\partial\mathbf{u}_{b,h}^F}{\partial\xi}\left(x^1(-1),y(\eta)\right)&=\sum_k u_{b,k}^F\frac{\partial\phi_{1,i}}{\partial\xi}(-1)\phi_{1,j}(\eta),\\ \frac{\partial\mathbf{u}_{b,h}^C}{\partial\xi}\left(x^0(1),y\left(\mu_m(\eta)\right)\right)&=\sum_k u_{b,k}^C\frac{\partial\phi_{0,i}}{\partial\xi}(1)\phi_{0,j}\left(\mu_m(\eta)\right).\end{aligned}\tag{41}$$

Then, the minimization statement of $\mathcal{J}^r_{m,1}$ is expressed as

$$\nabla \mathcal{J}^r_{m,1} = 0; \quad \mathbf{D}^T_{y,1}\mathbf{W}\mathbf{D}_{y,1}\mathbf{U}^F_{b,1} = \mathbf{D}^T_{y,1}\mathbf{W}\mathbf{D}_{ym,0}\mathbf{U}^C_{b,1}, \tag{42}$$

with

$$\begin{aligned} [\mathbf{D}_{y,1}]_{Q^2\times N} &= J_{x,1}\frac{\partial \phi_1}{\partial \xi}(-1) \otimes \phi_1(\eta_q), \\ [\mathbf{D}_{ym,0}]_{Q^2\times N} &= J_{x,0}\frac{\partial \phi_0}{\partial \xi}(1) \otimes \phi_0\left(\mu_m(\eta_q)\right), \quad q = 1, ..., Q. \end{aligned} \tag{43}$$

When $Q = p+1$, we can simplify Equation (42) by multiplying inverse matrices as

$$\mathbf{U}^F_{b,1} = \mathbf{D}^{-1}_{y,1}\mathbf{D}_{ym,0}\mathbf{U}^C_{b,1} \equiv \widetilde{\mathbf{Z}}_{m,1}\mathbf{U}^C_{b,1}, \tag{44}$$

with $\widetilde{\mathbf{Z}}_{m,1}$ the projection matrix for the derivative of solution value for the lower refined-element.

The expressions for the upper refined-element Ω^1_4 can be obtained in a similar way. Having established a relation between the unknowns of the finer and coarser elements at their inter-element borders, we can express the unknowns of the finer element $\mathbf{U}^F$ in terms of $\mathbf{U}^{F'}$, composed of the unknowns of the coarser element on the boarder and inner element unknowns $\mathbf{U}^F_i$ only:

$$\mathbf{U}^F = \begin{bmatrix} \mathbf{U}^F_{b,0} \\ \mathbf{U}^F_{b,1} \\ \mathbf{U}^F_i \end{bmatrix} = \begin{bmatrix} \widetilde{\mathbf{Z}}_0 & \mathbf{0} & \mathbf{0} \\ \mathbf{0} & \widetilde{\mathbf{Z}}_1 & \mathbf{0} \\ \mathbf{0} & \mathbf{0} & \mathbf{I} \end{bmatrix} \begin{bmatrix} \mathbf{U}^C_{b,0} \\ \mathbf{U}^C_{b,1} \\ \mathbf{U}^F_i \end{bmatrix} = \mathbf{Z}\mathbf{U}^{F'}, \tag{45}$$

where $\mathbf{Z}$ is the total projection matrix.

Implementation of these constraints into the least-square method can be performed by replacing the solution vector $\mathbf{U}$ as $\mathbf{U}^{'}$ using (45). The formulation at an element-level becomes

$$\mathbf{Z}^T_e\mathbf{L}^T_e\mathbf{W}_e\mathbf{L}_e\mathbf{Z}_e\mathbf{U}^{'}_e = \mathbf{Z}^T_e\mathbf{L}^T_e\mathbf{W}_e\mathbf{F}_e. \tag{46}$$

$\mathbf{Z}^T_e$ is additionally multiplied to maintain the symmetricity of the least-squares system.

4. Adaptive mesh refinement

4.1. Implementation

We design a systematic mesh refinement process. During the h-refinement an element is split into four daughter elements. An element with the refinement level k can be made by k-th mesh refinements from the original unrefined element. Each element is specified with two indices as Ω^k_i, where i and k indicate respectively the element number and the refinement level. Here we devise an element numbering system - 1) the elements are numbered in +x direction first

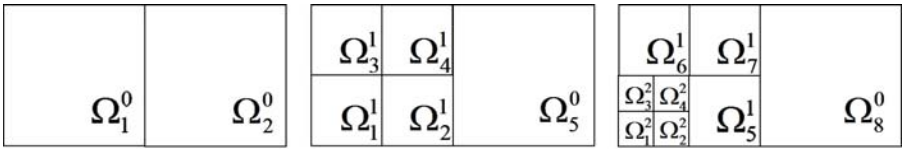

Figure 2: Examples of h-adaptivity with element numbering system and with 1-level irregularity.

and then +y direction, but 2) the numbering of the refined elements is done first inside the unrefined element in which they are. The grid system in Figure 2 is composed of the elements with level 0, 1 and 2, and it illustrates our element numbering system.

In this study, the maximum refinement level is set to 2, and we confine the irregularity up to 1-level, i.e., the difference in the refinement levels of neighboring elements is no larger than 1. All element configurations in Figure 2 satisfy the 1-level irregularity. The formulation of h-refinement can be simplified with the 1-level irregularity as an element has at most 2 neighbors along an edge. In addition, the 1-level irregularity can improve the accuracy in describing a sharp interface. The adjacent elements of level 2 elements are not marked by the refinement criteria, but their residual could be rather large. By the 1-level irregularity, these elements are refined in level 1 so that they give a transition zone. Fernandino et al. [22] showed the solution converged to a different steady state than physically predicted without a proper irregularity principle.

To reduce the computational memory usage for the refinement, we establish a lean data structure, revised from [23, 24]. The levels of each element are saved as an array, and the element numbers and the geometrical information are unsaved but calculated from this array. In addition, the location and configuration of elements are found by searching for which neighbors each element has. Unlike the conforming grid system, constructing the gathering matrix of basis functions in the non-conforming grid system requires more complicated steps. The basic element numbering is the same as the one of the conforming grid system, but here how to share the basis functions on the non-conformal element boarder is dependent on the configuration of the elements. If an element is neighboring with smaller or equal level of elements on its left or bottom side, it adopts the neighbor's basis functions which are non-zero on their element border. With this principle, all basis functions can be systematically numbered, except for four element configurations, as depicted in Figure 3. These configurations are automatically found by each specific conditions in the neighbor matrix, and their basis functions are reassigned.

4.2. Refinement criteria

The elements in the original unrefined grid are refined or retrieved at each time step depending on the result from the previous time step. Regarding the decision on which reference elements have to be refined, we consider two

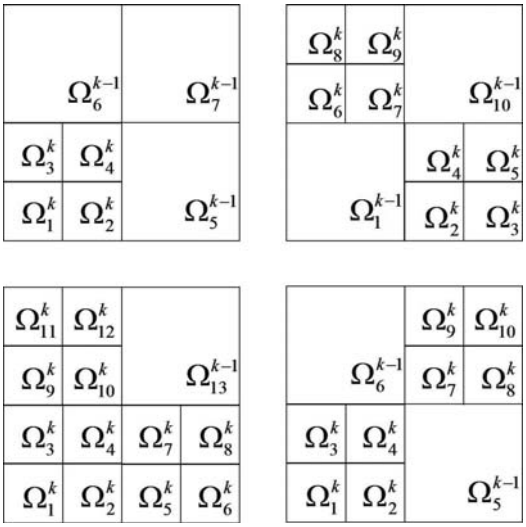

Figure 3: Element configurations which have to be considered separately in element numbering for element refinement level $k-1$ and k.

refinement criteria. With the first criterion (gradient), the elements where the solution gradients exceed a certain tolerance are refined, and it requires that

$$\|\nabla C\|^2_{0,\Omega_e} \leq tol_g, \tag{47}$$

with tol_g the discretization tolerance for the gradient. In the Cahn-Hilliard equation, it has been shown that the solution depends on the Cahn number which is a ratio of the interface thickness to the grid size [25]. The gradient criterion does not use any error estimator but it intensively targets to refine the interface.

The second criterion (residual) is the refinement of a fixed given number of elements based on the local residual in each element, defined as

$$\|\mathcal{R}\|^2_{0,\Omega_e} = \int_{\Omega_e} \left(\mathcal{L}\mathbf{u}^h - \mathcal{G}\right)^2 d\Omega_e. \tag{48}$$

Based on this, the reference elements are ordered in decreasing value of the local residual and the first elements are refined based on the specified percentage of elements given as refinement tolerance.

5. Numerical examples

For the Cahn-Hilliard equation, the equilibrium interface profile can be determined analytically as,

$$C_{eq} = \frac{1}{2} + \frac{1}{2} tanh\left(\frac{z}{2\sqrt{2}Cn}\right), \tag{49}$$

with the z-coordinate chosen along the gradient of the concentration. For the NSK system, the equilibrium interface profile for the density can be expressed as [15]:

$$\rho_{eq} = \frac{\rho_1 + \rho_2}{2} + \frac{\rho_1 - \rho_2}{2} tanh\left(\frac{z}{2}\sqrt{We}\right), \tag{50}$$

for the bulk densities $\rho_1 > \rho_2$. The initial concentration and density of all numerical simulations in the present article follow these equilibrium profiles. For the NSCH system, to assure the equilibrium state numerically as well, only the Cahn-Hilliard solver runs until the L^∞-norm of difference of concentration in time is lower than 10^{-4}, i.e., $max(C_{t=n+1} - C_{t=n}) < 10^{-4}$.

Both nonlinear and decoupling convergence are declared when the relative norm of the residual over the entire domain, i.e., $\|\Delta\mathcal{R}\|^2_{0,\Omega} \,/\, \|\mathcal{R}\|^2_{0,\Omega}$, is less than 10^{-6}, with the residual defined in (48) but over the entire domain Ω.

We display two coalescence examples driven by the NSCH and the isothermal NSK systems. The equilibrium state induced by the phase–field method has the minimum local free energy and surface tension energy, corresponding to the phase separation and the minimum interface length [3]. Since the coalescence examples accompany severe deformation of the interface, we can observe the changes of refinement grid depending on the evolution of the solution.

5.1. Coalescence driven by the NSCH system

Two bubbles with the same size are closely located, and they are coarsened by the diffusion without any external force. The initial concentration in a square domain $[0,1]^2$ is given as

$$\begin{aligned} C_0(\mathbf{x}) &= \frac{1}{2} + \frac{1}{2}\tanh\left(\frac{R - \|\mathbf{x} - \mathbf{x}_1\|}{2\sqrt{2}Cn}\right) \quad \text{for } \|\mathbf{x} - \mathbf{x}_1\| < \left(R + 2\sqrt{2}Cn\right), \\ C_0(\mathbf{x}) &= \frac{1}{2} + \frac{1}{2}\tanh\left(\frac{R - \|\mathbf{x} - \mathbf{x}_2\|}{2\sqrt{2}Cn}\right) \quad \text{for } \|\mathbf{x} - \mathbf{x}_2\| < \left(R + 2\sqrt{2}Cn\right), \end{aligned} \tag{51}$$

where radius R is 0.22 and $\|\|$ is the Euclidean distance between $\mathbf{x}$ and $\mathbf{x}_1 = (0.3333, 0.3333)$ or $\mathbf{x}_2 = (0.6667, 0.6667)$. For all simulation cases, the expansion order $p = 4$, the time step size $\Delta t = 0.1$ and the dimensionless numbers $Re = 400$, $Ca = 1$, $Pe = 100$, $Cn = 0.01$ are used. The initial grid is discretized with $Ne = 6^2$, and a conformal grid with $Ne = 24^2$ is also used for a comparison. As the refinement criteria, the gradient criterion with tol_g of 12.5 and the residual criterion with 45% and 62% of refined elements, corresponding the number of refined elements with the graident criterion at $t = 30.1$ and $t = 0.1$, are used.

The evolution of the concentration with the gradient criterion at $t = 0.1$, 5.1, 10.1 and 30.1 is presented in Figure 4. The interfacial area is successfully tracked to be refined with time. During the evolution, the total volume is completely conserved, more precisely that the volume loss is less than 10^{-5}% even if there is.

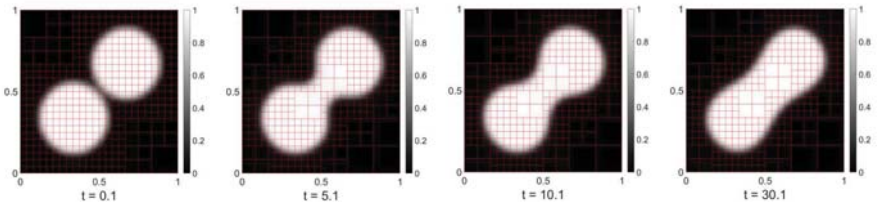

Figure 4: Evolution of concentration of coalescence driven by NSCH system on non–conformal grid with gradient criterion at $t = 0.1, 5.1, 10.1, 30.1$.

grid	Ndofs at $t = 10.1$	Total CPU hrs	CPU hrs in refinement
gradient	9,150 (63.5%)	53,541 (75.3%)	8,406 (15.7%)
residual 45%	7,950 (55.2%)	51,337 (72.2%)	8,419 (16.4%)
residual 62%	9,750 (67.7%)	59,656 (83.9%)	9,247 (15.5%)
conforming	14,400	71,104	

Table 1: Ndofs at $t = 10.1$, total CPU hours and CPU hours consumed in refinement procedure until $t = 10.1$ for gradient criterion, residual criterion of 45% and 62% and conforming grid. Percents in second and third column are values with respect to ones from confroming grid, and percent in fourth column is relative time consumption with respect to total CPU hours.

Figure 5 presents the concentration contour and the local residuals at $t = 10.1$ from the conformal grid and from the refined grids. The concentrations are almost identical regardless of the type of grids, but the refined elements and the local residuals are different. Overall, the residuals from the conformal grid is far smaller than the residual from the refined grids. The local residuals are symmetric in the cases of the gradient criterion and the conformal grid, while they are asymmetric with the cases of the residual criterion. The gradient criterion has a flexibility of the number of refined elements in time, because it is determined by the concentration. On the other hand, the number of refined elements with the residual criterion is fixed. As a result, the residual criterion sometimes yields asymmetric grid, and it manifests in the asymmetric local residuals. Note that here the local residual from the Navier–Stokes equations is negligible, of order under 10^{-5}, due to small velocity fields.

The number of degrees of freedom (Ndofs) at $t = 10.1$, total time consumption in CPU hours and time consumption for refinement procedures until $t = 10.1$ are provided in Table 1. With the refinement, we can reduce memory usage from 55.2% to 67.7%, and the computational hours from 72.2% to 83.9%. Around 16% of computational cost is spent in the refinement procedures, mainly in transferring the solution from the old to new refined grid in each time step, regardless of refinement strategies.

5.2. Coalescence driven by the isothermal NSK system

In this example, we solve the isothermal NSK system to simulate the coalescence of two droplets. This example has been handled in our previous study

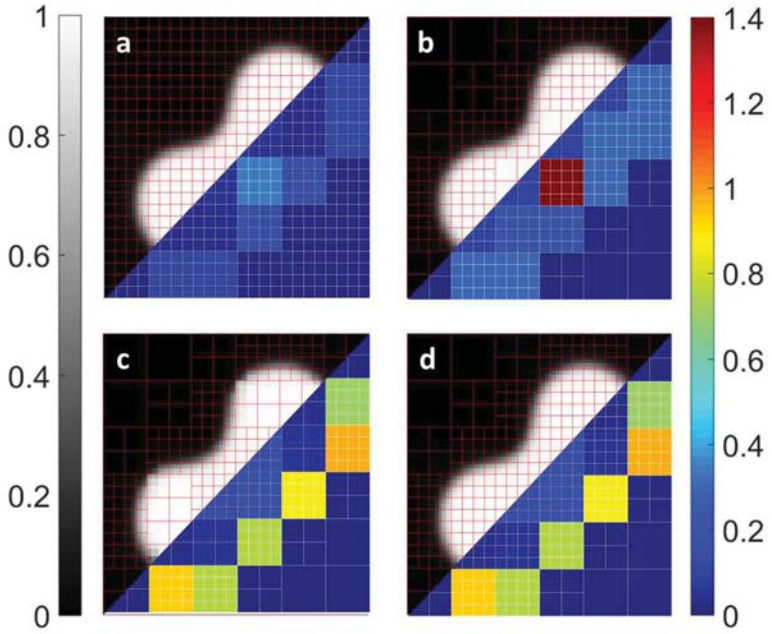

Figure 5: Concentration (top-left) local residual (bottom-right) on a) conformal grid and with b) gradient criterion and residual criterion of c) 45% and d) 62% of refined elements at $t = 10.1$.

[15] for a conformal grid. The initial density profile of two droplets in a spatial domain $\Omega_{\mathbf{x}} = [0, 1]^2$ is given as

$$\rho_0(\mathbf{x}) = \rho_l + \frac{\rho_l - \rho_v}{2}\left[\tanh\left(\frac{\|\mathbf{x} - \mathbf{x}_1\| - R_1}{2} \times \sqrt{We}\right) + \tanh\left(\frac{\|\mathbf{x} - \mathbf{x}_2\| - R_2}{2} \times \sqrt{We}\right)\right], \tag{52}$$

where $\rho_l = 1.810$ and $\rho_v = 0.3194$ are bulk densities of liquid and vapor at $\theta = 0.85$, the locations of droplets $\mathbf{x}_1 = (0.4, 0.5)$ and $\mathbf{x}_2 = (0.78, 0.5)$, and radii are set to be $R_1 = 0.25$ and $R_2 = 0.1$. The dimensionless parameters are fixed as $Re = 512$ and $We = 2000$, and all elements have the same expansion order $p = 4$. The initial reference grid is discretized with $Ne = 10^2$ elements, and it is refined only with the gradient criterion in this example with the tol_g of 13. Time step sizes vary as $\Delta t = 0.001, 0.0025, 0.005$. The results on the refined grid are compared with the one on the conformal grid $Ne = 40^2$ with $\Delta t = 0.005$.

Figure 6 presents the evolution of the density on the conformal grid and the non-conformal grid with $\Delta t = 0.005$. It is confirmed that the solutions are the

same regardless of the type of grid, and the gradient refinement criterion tracks the interfacial region to refine. For different time step sizes with the refined grid, the relative norms of the mass at $t = 0.855$ with respect to the initial mass $\mathcal{M}_0 = 0.6742$, named mass loss, i.e., $\|\mathcal{M}_{t=0.855} - \mathcal{M}_0\| \,/\, \|\mathcal{M}_0\|$, are presented in Table 2. The mass loss from the non-conformal grid is almost same or even a bit smaller than the one from the conformal grid for $\Delta t = 0.005$ case. And it is found that mass loss on the non-conformal grid is reduced as decreasing the time step size, and this result corresponds to our previous study for the conformal grid [15].

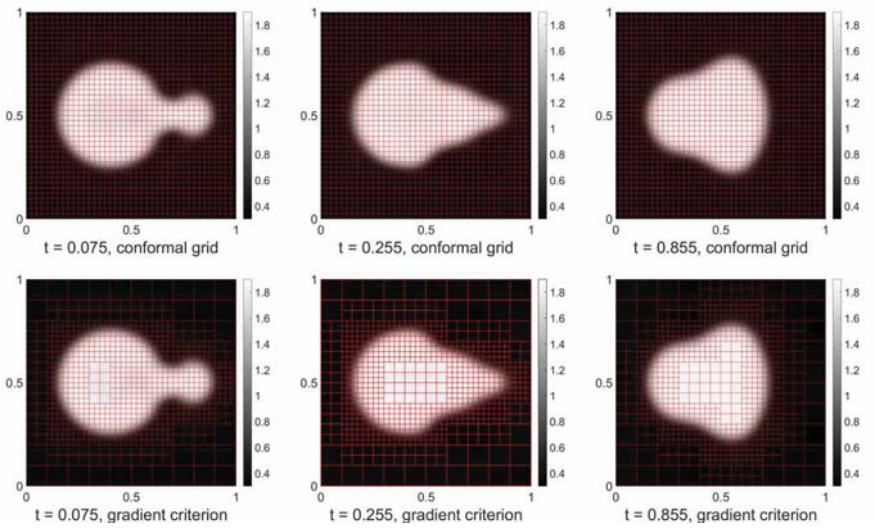

Figure 6: Evolution of density of coalescence driven by isothermal NSK system on conformal grid (top) and on non–conformal grid with gradient criterion (bottom), with $\Delta t = 0.005$ and at $t = 0.075, 0.255, 0.855$.

grid type	non-conformal			conformal
time step size	$\Delta t = 0.001$	$\Delta t = 0.0025$	$\Delta t = 0.005$	$\Delta t = 0.005$
$\frac{\|\mathcal{M}_{t=0.855} - \mathcal{M}_0\|}{\|\mathcal{M}_0\|}$	5.93×10^{-5}	1.33×10^{-4}	2.67×10^{-4}	3.11×10^{-4}

Table 2: Mass loss at $t = 0.855$ from non-conformal grid with $\Delta t = 0.001, 0.0025, 0.005$ and from conformal grid with $\Delta t = 0.005$.

6. Concluding remarks

We presented a C^1 continuous h-adaptive least-squares spectral element method for the Navier-Stokes-Cahn-Hilliard (NSCH) system and the isother-

mal Navier-Stokes-Korteweg (NSK) system as the representatives of the phase-field models. To provide the global differentiability of the solution, C^1 Hermite polynomials were used as basis functions, and the corresponding refinement procedures were provided. Two refinement strategies based on the solution gradient and the local residual were considered, and their performances were compared through the numerical examples. The results from the refined grid were validated by comparing with the results from the conformal grid. With an example of coalescence driven by the NSCH system, we found the gradient criterion gives us more stable and predictable results, because it targets only interface elements. On the other hand, the residual criterion results in asymmetric local residual map because of its rigidity on the number of refined elements. However, the one of the greatest advantages of least-squares method is that the functional provides a natural error measure, which no other methods possesses [16]. To enjoy this advantage, we can consider in the future to refine elements based on the gradient criterion but support it by refining other elements if their residuals are above a certain level. With the refinement technique, we reduced both memory usage and computational cost, and it was found that the percentages of the computational cost spent in the refinement procedures with respect to the total cost are not very different depending on the refinement criteria. In the coalescence driven by the isothermal NSK system, a parametric study on the time step size was conducted with the gradient criterion. The mass loss with the refined grid was almost the same as the one with the conformal grid if the same time step size was used. And the mass loss is reduced as decreasing the time step size, and this result corresponds to our previous study on the conformal grid [15].

Acknowledgements

Funding for this work from the Research Council of Norway under the FRINATEK project 214424 is gratefully acknowledged.

References

[1] P. Yue, C. Zhou, J.J. Feng,C.F. Ollivier–Gooch, H.H. Hu, Phase–field simulations of interfacial dynamics in viscoelastic fluids using finite elements with adaptive meshing, J. Comput. Phys., 219 (2006) 47–67.

[2] M. Fernandino, C.A. Dorao, The least squares spectral element method for the Cahn-Hilliard equation, Appl. Math. Mod. 35 (2011) 797–806.

[3] J.W. Cahn, J.E. Hilliard, Free energy of a nonuniform system. I. Interfacial free energy, J. Chem. Phys. 28 (1958) 258–267.

[4] J.S. Rowlinson, The thermodynamic theory of capillarity under the hypothesis of a continuous variation of density (Translation of JD van der Waals, J. Stat. Mech. 28 (1979) 197.

[5] M.P. Dupuy, M. Fernandino, H.A. Jakobsen, H.F. Svendsen, Fractional step two-phase flow lattice Boltzmann model implementation, J. Stat. Mech. P06014 (2009).

[6] D. Derks, D.G.A.L. Aarts, D. Bonn, A. Imhof, Phase separating colloid polymer mixtures in shear flow, J. Phys. Condens. Matter 20 (2008) 412–416.

[7] T. Hashimoto, K. Matsuzaka, E. Moses, A. Onuki, String phase in phase–separating fluids under shear flow, Phys. Rev. Lett. 74 (1995) 126–129.

[8] J.A. Warren, W.J. Boettinger, Prediction of dendritic growth and microsegregation patterns in a binary alloy using the phase–field method, Acta Mater. 43 (1995) 689–703.

[9] P.C. Hohenberg, B.I. Halperin, Theory of dynamic critical phenomena, Rev. Mod. Phys. 49 (1977) 435.

[10] D.J. Korteweg, Sur la forme que prennent les equations du mouvement des fluides si lon tient compte des forces capillaires causees par des variations de densite considerables mais continues et sur la theorie de la capillarite dans lhypothese dune variation continue de la densite, Archives Nerlandaises des Sciences exactes et naturelles 6 (1901) 6.

[11] M. Rimboud, R.D. Hart, T. Becker, D.W. Arrigan, Electrochemical behaviour and voltammetric sensitivity at arrays of nanoscale interfaces between immiscible liquids, Analyst 136 (2011) 4674–4681.

[12] D. Diehl, Higher order schemes for simulation of compressible liquid–vapor flows with phase change, PhD thesis, Universitat Freiburg.

[13] I. Barosan, Adaptive spectral elements for diffuse interface multi-fluid flow, PhD thesis, Technische Universiteit Eindhoven.

[14] K. Park, M. Fernandino, C.A. Dorao, Numerical Solution of Incompressible Cahn–Hilliard and Navier–Stokes System with Large Density and Viscosity Ratio Using the Least-Squares Spectral Element Method, J. Fluid Flow, Heat & Mass Transfer 43 (1995) 689–703.

[15] K. Park, M. Fernandino, C.A. Dorao, M. Gerritsma, The least–squares spectral element method for phase–field models for isothermal fluid mixture, Comput. Math. Appl. (submitted).

[16] B. Jiang, The Least–Square Finite Element Method: Theory and Applications in Computational Fluid Dynamics and Electromagnetics, Springer, Berlin, 2013.

[17] P.B. Bochev, M.D. Gunzburger, Least–squares finite element methods, 166 Springer, New York, 2009.

[18] C. Carstensen, M. Feischl, M. Page, D. Praetorius, Axioms of adaptivity, Comput. Math. Appl. 67 (2014) 1195–1253.

[19] R.H. Stogner, F.C. Graham, T.M. Bruce, Approximation of Cahn-Hilliard diffuse interface models using parallel adaptive mesh refinement and coarsening with C1 elements, Int. J. Numer. Meth. Eng. 76 (2008) 636–661.

[20] K. Park, C.A. Dorao, M. Fernandino, Numerical solution of coupled Cahn–Hilliard and Navier–Stokes system using the least-squares spectral element method, ASME 2016 14th International Conference on Nanochannels, Microchannels, and Minichannels (2016).

[21] P. Solin, K. Segeth, Towards optimal shape functions for hierarchical Hermite elements, in Proceedings of the SANM conference, Srni, Czech Republic (2005).

[22] M. Fernandino, N.L. Forgia, Refinement strategies for the Cahn–Hilliard equation using the least squares method, MekIT13, 13-14 May, Trondheim, Norway (2011).

[23] J. Wackers, B. Koren, A simple and efficient space–time adaptive grid technique for unsteady compressible flows, in 16th AIAA Computational Fluid Dynamics Conference (2003).

[24] A. Galvao, M. Gerritsma, B. De Maerschalck, hp–Adaptive least squares spectral element method for hyperbolic partial differential equations, J. Comput. Appl. Math. 215 (2008) 409–418.

[25] Y.J. Choi, P.D. Anderson, Cahn–Hilliard modeling of particles suspended in two-phase flows, Int. J. Numer. Meth. Fluids 69 (2012) 995–1015.

[26] D. Kay, V. Styles, R. Welford, Finite element approximation of a Cahn–Hilliard–Navier–Stokes system, J. Hydraul. Eng. 123 (1997) 41–50.

[27] T. Komatsu, K. Ohgushi, K. Asai, Refined numerical scheme for advective transport in diffusion simulation, Interface Free Bound 10 (2008) 15–43.